IEEE Access
Multidisciplinary | Rapid Review | Open Access Journal

Received March 14, 2021, accepted March 20, 2021, date of publication March 24, 2021, date of current version April 1, 2021.

Digital Object Identifier 10.1109/ACCESS.2021.3068813

State-of-Charge and State-of-Health Estimation for Lithium-Ion Batteries Based on Dual Fractional-Order Extended Kalman Filter and Online Parameter Identification

LIUYI LING[1,2] AND YING WEI[3]

[1]School of Artificial Intelligence, Anhui University of Science and Technology, Huainan 232001, China
[2]School of Electrical and Information Technology, Anhui University of Science and Technology, Huainan 232001, China
[3]School of Electronic and Electrical Engineering, Anhui Sanlian University, Hefei 230601, China

Corresponding authors: Liuyi Ling (lyling@aust.edu.cn) and Ying Wei (weiying8ths@sohu.com)

This work was supported by the Project of the Natural Science Foundation of the Higher Education Institute of Anhui Province under Grant KJ2019A0106.

ABSTRACT Accurate state-of-charge (SOC) and state-of-health (SOH) estimations of batteries are of great significance for electric vehicles. A combined SOC and SOH estimation method for lithium-ion batteries based on a dual extended Kalman filter (EKF) and fractional-order model (FOM) is proposed. A fractional second-order RC model is established and model parameters are identified offline by an adaptive genetic algorithm (AGA). One of the dual filters is used to jointly estimate the SOC and SOH (ohmic internal resistance and capacity), and another is employed to update the model parameters online. Compared with single filter with fixed parameters, the dual filters can obtain more accurate SOC estimation and model voltage prediction. The SOC root-mean square errors (RMSEs) decrease from 6.87%, 8.50% and 7.32% to 0.48%, 0.63% and 0.86% under the Federal Urban Driving Schedule (FUDS), the Dynamic Stress Test (DST) and the US06 Highway Driving Schedule tests, respectively, and the model voltage RMSEs decrease from 88.6 mV, 79.3 mV and 68.4 mV to 4.9 mV, 5.7 mV and 3.8 mV, respectively at room temperature. The accuracy of the SOH estimation is also verified under these three tests. The convergence and robustness of the proposed method are discussed and verified by using the wrong initial state value and noise analysis.

INDEX TERMS State-of-charge, state-of-health, lithium-ion battery, fractional-order model, dual Kalman filter.

I. INTRODUCTION

Owing to the merits of high energy density, long cycle life and no memory effect, lithium-ion batteries have been widely used in electric vehicles (EV). Pure batteries or battery-supercapacitor hybrids have been regarded as an alternative to traditional fossil fuels [1]. A battery system in EV often consists of a certain number of series-parallel connected battery cells to meet the voltage and capacity requirements. Reliable and efficient battery management system (BMS) is critical due to users' ever-increasing concerns on the safety and consistency for battery packs [2]. As two key states in BMS, state of charge (SOC) and state of health (SOH) not only define the safety margin of battery to avoid overcharge or overdischarge, but also help to make full utilization of battery capacity potential. The battery SOC is commonly defined as the ratio of remaining capacity to actual capacity. The battery SOH can be described by either ohmic internal resistance or actual capacity. Unfortunately, neither SOC nor SOH can be measured directly and they have to be estimated by employing advanced algorithms with the use of measurable quantities, such as current, voltage and temperature.

Several SOC estimation methods have been proposed in the literature [3]–[5]. The coulomb counting method is easily implemented and the most commonly used in realistic BMSs. However, its accuracy highly depends on the precision of the current sensors and the accuracy of initial SOC value, which results in the accumulated error over time. The open-circuit

The associate editor coordinating the review of this manuscript and approving it for publication was Yanbo Chen.

voltage (OCV) method can be used to estimate the SOC, but not suitable for real time estimation since accurate measurement of the OCV requires that the battery has achieved a stabilized status, which generally needs several hours. Purely data-driven algorithms, such as neural networks [6]–[9], support vector machines [10], and fuzzy logic [11], are also used to predict the battery SOC. However, the accuracy of SOC prediction highly rely on the quantity and quality of training datasets, hence these techniques generally cannot extrapolate to conditions beyond those outside the training datasets. Model-based SOC estimation methods are promising for real applications since they have advantages of closed loop self-correction and online implementations. Specifically, equivalent circuit model (ECM) is more favorable due to the simplicity and sufficiency for emulating the battery dynamics. Based on ECM, a number of observers have been proposed for SOC estimation, for example sliding mode observer [12], H-infinity observer [13], particle filter [14] and Kalman filter family [15]–[17]. Such works use static models where model parameters are identified offline and assumed to be unchanged over time. Although these observers can obtain accurate SOC values under specific conditions, the SOC estimation could produce large errors under other working conditions, because these offline identified parameters are not necessarily suitable for such conditions.

On the other hand, for SOH estimation, data-driven approaches and many of the aforementioned observers were applied to predict battery aging level or were coupled or extended to concurrently estimate SOC and SOH. For example, She *et al.* [18] presented a radial basis function neural network model for battery aging assessment. The model has high prediction accuracy owing to training datasets collected from real-world electric city buses. In Ref. [19], a fourth-order extended Kalman filter (EKF) was employed for joint estimation of SOC and SOH. However, the SOH estimator was only triggered when SOC estimation and modeling errors become unacceptable, thus it was operated offline. To achieve synchronously online estimation of the battery SOC and SOH, some dual Kalman filter algorithms were proposed. In Ref. [20], SOC and SOH under battery degradation was estimated using a dual EKF. However, its estimation accuracy may not be maintained if ambient temperature varies since the parameters of the ECM are identified offline except internal resistance. The method presented in Ref. [21] adopted a dual EKF combining with adaptive algorithm for correcting noise variance to estimate SOH as well as SOC of airborne lithium-ion batteries. Although ohmic internal resistance and capacity were online estimated, other parameters of the model were fixed, which could result in large estimation error if there was a big difference between actual working and test conditions. In Ref. [22], online parameter identification, and SOC and ohmic internal resistance joint estimation were implemented by using a multitimescale double KF. By updating model parameters online, the accuracy of SOC estimation was improved. However, the integer-order components used in the adopted circuit model are not sufficient to depict the highly nonlinear effects of the battery, which limits the accuracy.

Recently, fractional-order calculus has been widely used in battery modeling. Xiao *et al.* [23] established a fractional order model (FOM) for SOC estimation, compared the performance of the FOM and integer order model (IOM), and found that the FOM can simulate the battery terminal voltage variation more precisely, and the SOC estimation based on the FOM was more accurate. In Refs [24]–[26], multiple SOC estimation schemes based on FOMs have also been researched for lithium-ion batteries, exhibiting satisfactory results. Considering the advantages of FOM, Xu *et al.* [27] designed a FOM-based double Kalman filter for estimating the battery SOC and updating ohmic internal resistance by using recursive least squares method. However, other parameters of the FOM were fixed, in other words, influence of the variations of these parameters caused by SOC, working conditions or temperature on SOC was ignored. Likewise, in Ref. [28], only ohmic internal resistance in the FOM as well as the battery capacity is estimated online. In Ref. [29], only the fractional orders were estimated online, while other parameters were identified offline. Investigation results of Ref. [30] reveal that each fractional-order parameter has its own influence with a different degree of sensitivity on the model output accuracy. Therefore, in order to make full use of the advantages of FOM, each parameter in the model should be estimated online. However, to the best of our knowledge, there is a lack of studies on joint estimation of the battery SOC and SOH base on online identification of each parameter of FOM.

In order to overcome the drawbacks mentioned above, this paper proposes a novel estimation method based on dual fractional-order extended Kalman filter and online parameter identification. The dual estimation scheme is designed to estimate the SOC as well as SOH (ohmic internal resistance and capacity) and synchronously update each parameter of the fractional-order model online. The main contributions of this work include: 1) We use fractional calculus to model the battery and all the model parameters are identified online, which can ensure the accuracy of the modeling no matter what working condition the battery is operated in; 2) We give the strict calculation process of dual fractional-order extended Kalman filter algorithm for joint estimation of SOC and SOH; 3) The accuracy of the proposed method is verified under the Federal Urban Driving Schedule (FUDS), the Dynamic Stress Test (DST) and the US06 Highway Driving Schedule at different temperatures. Its convergence and robustness are discussed and verified by using the wrong initial state value and noise analysis.

The rest of this paper is organized as follows. Section II describes fractional-order battery modeling after briefing fundamentals of fractional order calculus. The state estimation and online parameter identification method based on dual fractional-order EKF is presented in Section III. Section IV describes experimental data and offline parameter identification. Experimental results used to verify the accuracy,

convergence and robustness of the proposed method are discussed in Section V. Finally, the conclusion is presented in Section VI.

II. FRACTIONAL-ORDER BATTERY MODELING

A. FUNDAMENTALS OF FRACTIONAL ORDER CALCULUS

Three most frequently used definitions of fractional calculus are the Caputo definition, the Riemann-Liouville definition and the Grünwald–Letnikov (GL) definition [31]. The GL definition depicts discretization of the continuous fractional-order equations and hence is very suitable for numerical calculation. In addition, it is concise and easy to combine with Kalman filtering techniques. Therefore, we use the GL definition to establish fractional-order equations for the battery FOM. The GL fractional-order derivative of non-integer order α is defined as

$$\mathcal{D}^{\alpha}x(t) = \lim_{h\to 0}\frac{1}{h^{\alpha}}\sum_{j=0}^{[t/h]}(-1)^{j}\binom{\alpha}{j}x(t-jh), \tag{1}$$

$$\binom{\alpha}{j} = \begin{cases} 1 & j=0 \\ \dfrac{\alpha(\alpha-1)\cdots(\alpha-(j-1))}{j!} & j>0, \end{cases} \tag{2}$$

where $\mathcal{D}$ is the differential operator, α is the differential order value, h is the sample time and $[t/h]$ represents the integer part of t/h.

B. FRACTIONAL-ORDER MODEL FOR LITHIUM-ION BATTERIES

Considering that the second-order RC circuit has high precision and moderate parameter number, we establish a fractional second-order RC circuit to model the battery in this study. The model is constructed as shown in Fig. 1.

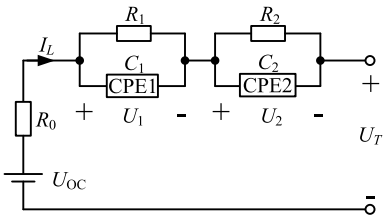

FIGURE 1. Schematic diagram of the fraction-order battery model.

For the FOM model, the mathematical relationship between the current and the voltage can be expressed as:

$$\begin{cases} \mathcal{D}^{\alpha}U_1 = -\dfrac{1}{R_1C_1}U_1 + \dfrac{1}{C_1}I_L \\ \mathcal{D}^{\beta}U_2 = -\dfrac{1}{R_2C_2}U_2 + \dfrac{1}{C_2}I_L, \end{cases} \tag{3}$$

$$U_T = U_{OC} - R_0I_L - U_1 - U_2 \tag{4}$$

where U_1 and U_2 denote the voltage of the constant phase element (CPE1) and CPE2, U_{T} and I_{L} are terminal voltage and load current, U_{OC} represents the open circuit voltage, the R_0 is the ohmic internal resistance, and R_1, C_1, R_2, and C_2 denote the electrochemical polarization resistance and capacitance, and the concentration polarization resistance and capacitance. The α and β are the differentiation orders of the two CPEs, $0 < \alpha, \beta \leq 1$. When $\alpha = \beta = 1$, the model turns into integer order model.

According to the FOC definition in Eq. (1), Eq. (3) can be discretized as the following equation:

$$\begin{cases} \dfrac{1}{T_S^{\alpha}}\displaystyle\sum_{j=0}^{k}(-1)^{j}\binom{\alpha}{j}U_{1,k-j} = \dfrac{1}{C_1}I_{L,k-1} \\ \qquad\qquad -\dfrac{1}{R_1C_1}U_{1,k-1}, \\ \dfrac{1}{T_S^{\beta}}\displaystyle\sum_{j=0}^{k}(-1)^{j}\binom{\beta}{j}U_{2,k-j} = \dfrac{1}{C_2}I_{L,k-1} \\ \qquad\qquad -\dfrac{1}{R_2C_2}U_{2,k-1}, \end{cases} \tag{5}$$

where T_S is the sample time. It should be noted that the sum of the items include all the past states before the current time step k. As the number of the items becomes large, the computation burden increases. In real application, considering the accuracy requirement for the battery model, computation burden and the short-term memory principle [32], the summing item can be appropriately truncated. The summing upper bound is set to be one in this study. Then, Eq. (5) can be modified as:

$$\begin{cases} U_{1,k} = (\alpha - \dfrac{T_S^{\alpha}}{R_1C_1})U_{1,k-1} + \dfrac{T_S^{\alpha}}{C_1}I_{L,k-1}, \\ U_{2,k} = (\beta - \dfrac{T_S^{\beta}}{R_2C_2})U_{2,k-1} + \dfrac{T_S^{\beta}}{C_2}I_{L,k-1}. \end{cases} \tag{6}$$

According to the battery SOC calculation by the coulomb counting method, one can acquire:

$$SOC_k = SOC_{k-1} - \frac{\eta T_S}{C_{\mathrm{p}}}I_{L,k-1}, \tag{7}$$

where η is the charge-discharge efficiency and C_{p} is the nominal battery capacity.

The terminal voltage can be expressed as

$$U_{T,k} = U_{OC,k} - U_{1,k} - U_{2,k} - R_0I_{L,k}. \tag{8}$$

In Eq. (8), the open-circuit voltage $U_{OC,k}$ can be replaced by the function $OCV(SOC_k)$ with respect to SOC_k; furthermore, this function can be approximately expressed as a linear function by using a first-order Taylor expansion.

To accurately describe the battery behavior under different working conditions, the indicator of battery SOH, i.e. the actual capacity C_{p} and R_0 in Eq. (7) and (8), and the parameters of the fraction-order battery model, namely, R_1, C_1, R_2, C_2 and the differentiation order α and β in Eq. (6), should be online estimated. Considering that the actual capacity C_{p} and R_0 vary slowly as the battery cell ages, by defining $x_k = [SOC_k, U_{1,k}, U_{2,k}, R_{0,k}, 1/C_{\mathrm{p},k}]^{\mathrm{T}}$, $u_k = I_{L,k}$, $y_k = U_{T,k}$,

$\theta_k = [1/R_{1,k}, 1/C_{1,k}, \alpha_k, 1/R_{2,k}, 1/C_{2,k}, \beta_k]^{\mathrm{T}}$, therefore the model (6)-(8) can be rewritten as

$$\begin{aligned} x_k &= A(\theta_{k-1})\, x_{k-1} + B(\theta_{k-1})\, u_{k-1} \\ &= f(x_{k-1}, u_{k-1}, \theta_{k-1}), \end{aligned} \tag{9}$$

$$\begin{aligned} y_k &= OCV(x_{1,k}) - x_{2,k} - x_{3,k} - x_{4,k} u_k \\ &= g(x_k, u_k, \theta_k), \end{aligned} \tag{10}$$

where

$$A(\theta_k) = \begin{bmatrix} 1 & 0 & 0 & 0 & -\eta T_S u_k \\ 0 & \theta_{3,k} - \theta_{1,k}\theta_{2,k} T_S^{\theta_{3,k}} & 0 & 0 & 0 \\ 0 & 0 & \theta_{6,k} - \theta_{4,k}\theta_{5,k} T_S^{\theta_{6,k}} & 0 & 0 \\ 0 & 0 & 0 & 1 & 0 \\ 0 & 0 & 0 & 0 & 1 \end{bmatrix},$$

$$B(\theta_k) = \begin{bmatrix} 0 \\ \theta_{2,k} T_S^{\theta_{3,k}} \\ \theta_{5,k} T_S^{\theta_{6,k}} \\ 0 \\ 0 \end{bmatrix},$$

$x_{i,k}$ denotes the ith element of x_k, and $\theta_{i,k}$ represents the ith element of θ_k.

III. DFOEKF FOR JOINT ESTIMATION OF SOC/SOH AND ONLINE PARAMETER IDENTIFICATION

In this paper, the ohmic internal resistance and the capacity are used to characterize the battery SOH. In order to achieve online parameter identification and joint estimation of the SOC and SOH, a dual fractional-order extended Kalman filtering (DFOEKF) algorithm is proposed. The first filter, FOEKF^x, estimates the SOC and SOH state, x_k, and the second filter, FOEKF$^\theta$, synchronously estimates the parameter state,θ_k. The DFOEFK algorithm jointly estimates the SOC as well as the SOH and updates the battery model parameters. The proposed DFOEFK algorithm is schematically shown in Fig. 2. It can be seen that both estimators exchange information recursively at each step. The implementation of FOEKF^x and FOEKF$^\theta$ is presented in section III-A and III-B.

A. THE FIRST FOEKF FOR CO-ESTIMATION OF THE SOC AND SOH

The calculation process of the first FOEKF for the battery SOC and SOH estimation can be formulated by the following equations.

State equation:

$$x_{k+1} = f(x_k, u_k, \theta_k) + w_k^x. \tag{11}$$

Measurement equation:

$$y_k = g(x_k, u_k, \theta_k) + v_k^x, \tag{12}$$

where w_k^x and v_k^x denote the state noise and the measurement noise for state vector x, respectively. They are the independent white noise with zero mean and their variances are Q_k^x and R_k^x, respectively, which are determined by trial and error.

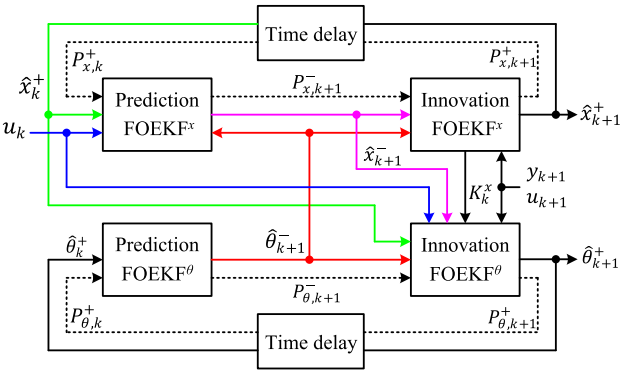

FIGURE 2. Schematic of the proposed dual fractional-order extended kalman filter for state and parameter synchronous estimation.

Prediction of the state vector x:

$$\hat{x}^-_{k+1} = f\left(\hat{x}^+_k, u_k, \hat{\theta}^-_{k+1}\right), \tag{13}$$

where $\hat{\theta}^-_{k+1}$ is prediction of the parameter θ from the second FOEKF and $\hat{x}^+_k$ denotes the posterior estimate of x at time k.

Prediction of the estimate error variance:

$$P^-_{x,k+1} = A\left(\hat{\theta}^-_{k+1}\right) P^+_{x,k} \left(A\left(\hat{\theta}^-_{k+1}\right)\right)^{\mathrm{T}} + Q^x_k, \tag{14}$$

where $P^+_{x,k}$ is the posterior estimate of the estimate error variance at time k.

Kalman gain matrix calculation:

$$K^x_k = P^-_{x,k+1}(H^x_k)^{\mathrm{T}} \left(H^x_k P^-_{x,k+1}(H^x_k)^{\mathrm{T}} + R^x_k\right)^{-1}, \tag{15}$$

where H^x_k is the Jacobian matrix and can be expressed as

$$\begin{aligned} H^x_k &= \left.\frac{\partial g(\cdot)}{\partial x_k}\right|_{x_k = \hat{x}^-_{k+1}} \\ &= \left[\left.\frac{\partial OCV(SOC)}{\partial SOC}\right|_{SOC = \hat{x}^-_{1,k+1}}, -1, -1, -u_k, 0\right]. \end{aligned} \tag{16}$$

Update of the state vector x:

$$\hat{x}^+_{k+1} = \hat{x}^-_{k+1} + K^x_k \left(y_k - g\left(\hat{x}^-_{k+1}, u_k, \hat{\theta}^-_{k+1}\right)\right). \tag{17}$$

Update of the estimate error variance:

$$P^+_{x,k+1} = \left(I - K^x_k H^x_k\right) P^-_{x,k+1}, \tag{18}$$

where I is the unit matrix.

B. THE SECOND FOEKF FOR ONLINE PARAMETER IDENTIFICATION

Unlike the battery SOC, the model parameter is slow-varying variable. Therefore, the parameter vector θ_k is regarded as constant and disrupted by the state noise only. The calculation process of the second FOEKF for online parameter identification can be formulated by the following equations.

State equation:

$$\theta_{k+1} = \theta_k + w_k^{\theta}. \tag{19}$$

Measurement equation:

$$y_k = g\left(x_k, u_k, \theta_k\right) + v_k^{\theta}, \tag{20}$$

where w_k^{θ} and v_k^{θ} denote the state noise and the measurement noise for vector θ, respectively. They are the independent white noise with zero mean and their variances are Q_k^{θ} and R_k^{θ}, respectively.

Prediction of the state vector θ:

$$\hat{\theta}_{k+1}^{-} = \hat{\theta}_k^{+}, \tag{21}$$

where $\hat{\theta}_k^{+}$ denotes the posterior estimate of θ at time k.

Prediction of the estimate error variance:

$$P_{\theta,k+1}^{-} = P_{\theta,k}^{+} + Q_k^{\theta}, \tag{22}$$

where $P_{\theta,k}^{+}$ is the posterior estimate of the estimate error variance at time k.

Kalman gain matrix calculation:

$$K_k^{\theta} = P_{\theta,k+1}^{-}(H_k^{\theta})^{\mathrm{T}}\left(H_k^{\theta}P_{\theta,k+1}^{-}(H_k^{\theta})^{\mathrm{T}} + R_k^{\theta}\right)^{-1}. \tag{23}$$

Update of the state vector θ:

$$\hat{\theta}_{k+1}^{+} = \hat{\theta}_{k+1}^{-} + K_k^{\theta}\left(y_k - g\left(\hat{x}_{k+1}^{-}, u_k, \hat{\theta}_{k+1}^{-}\right)\right). \tag{24}$$

Update of the estimate error variance:

$$P_{\theta,k+1}^{+} = \left(I - K_k^{\theta}H_k^{\theta}\right)P_{\theta,k+1}^{-}, \tag{25}$$

where I is the unit matrix.

In Eq. (23) and (25), H_k^{θ} is the Jacobian matrix and need to be carefully calculated. In order to easily understand the calculate process, we list the expressions of functions $f(\cdot)$ and $g(\cdot)$ again.

Notablely, in this paper, the sample time, T_S, is 1 s, hence both factors, $T_S^{\theta_{3,k}}$ and $T_S^{\theta_{6,k}}$ in Eq. (26), as shown at the bottom of the page, have the value of one. For simplicity, the efficiency η is set to one. The calculation process of H_k^{θ} can be formulated by the following equations.

$$H_k^{\theta} = \left.\frac{dg\left(\hat{x}_{k+1}^{-}, u_{k+1}, \theta_k\right)}{d\theta_k}\right|_{\theta_k=\hat{\theta}_{k+1}^{-}}, \tag{28}$$

$$\frac{dg\left(\hat{x}_{k+1}^{-}, u_{k+1}, \theta_k\right)}{d\theta_k} = \frac{\partial g\left(\hat{x}_{k+1}^{-}, u_{k+1}, \theta_k\right)}{\partial\theta_k} + \frac{\partial g\left(\hat{x}_{k+1}^{-}, u_{k+1}, \theta_k\right)}{\partial\hat{x}_{k+1}^{-}} \cdot \frac{d\hat{x}_{k+1}^{-}}{d\theta_k}, \tag{29}$$

$$\frac{\partial g\left(\hat{x}_{k+1}^{-}, u_{k+1}, \theta_k\right)}{\partial\theta_k} = [0, 0, 0, 0, 0, 0], \tag{30}$$

$$\frac{\partial g\left(\hat{x}_{k+1}^{-}, u_{k+1}, \theta_k\right)}{\partial\hat{x}_{k+1}^{-}} = \left[\left.\frac{\partial OCV(SOC)}{\partial SOC}\right|_{SOC=\hat{x}_{1,k+1}^{-}}, -1, -1, -u_{k+1}, 0\right]. \tag{31}$$

Next, we calculate $\frac{d\hat{x}_{k+1}^{-}}{d\theta_k}$ and define it as D_k^{θ}. (32)–(34), as shown at the bottom of the page.

$$f\left(x_k, u_k, \theta_k\right) = \begin{bmatrix} 1 & 0 & 0 & 0 & -\eta T_S u_k \\ 0 & \theta_{3,k} - \theta_{1,k}\theta_{2,k}T_S^{\theta_{3,k}} & 0 & 0 & 0 \\ 0 & 0 & \theta_{6,k} - \theta_{4,k}\theta_{5,k}T_S^{\theta_{6,k}} & 0 & 0 \\ 0 & 0 & 0 & 1 & 0 \\ 0 & 0 & 0 & 0 & 1 \end{bmatrix} x_k + \begin{bmatrix} 0 \\ \theta_{2,k}T_S^{\theta_{3,k}} \\ \theta_{5,k}T_S^{\theta_{6,k}} \\ 0 \\ 0 \end{bmatrix} u_k, \tag{26}$$

$$g\left(x_k, u_k, \theta_k\right) = OCV\left(x_{1,k}\right) - x_{2,k} - x_{3,k} - x_{4,k}u_k. \tag{27}$$

$$D_k^{\theta} = \frac{d\hat{x}_{k+1}^{-}}{d\theta_k} = \frac{\partial f\left(\hat{x}_k^{+}, u_k, \theta_k\right)}{\partial\theta_k} + \frac{\partial f\left(\hat{x}_k^{+}, u_k, \theta_k\right)}{\partial\hat{x}_k^{+}} \cdot \frac{d\hat{x}_k^{+}}{d\theta_k}, \tag{32}$$

$$\frac{\partial f\left(\hat{x}_k^{+}, u_k, \theta_k\right)}{\partial\theta_k} = \begin{bmatrix} 0 & 0 & 0 & 0 & 0 & 0 \\ -\hat{x}_{2,k}^{+}\hat{\theta}_{2,k+1}^{-} & u_k - \hat{x}_{2,k}^{+}\hat{\theta}_{1,k+1}^{-} & \hat{x}_{2,k}^{+} & 0 & 0 & 0 \\ 0 & 0 & 0 & -\hat{x}_{3,k}^{+}\hat{\theta}_{5,k+1}^{-} & u_k - \hat{x}_{3,k}^{+}\hat{\theta}_{4,k+1}^{-} & \hat{x}_{3,k}^{+} \\ 0 & 0 & 0 & 0 & 0 & 0 \\ 0 & 0 & 0 & 0 & 0 & 0 \end{bmatrix}, \tag{33}$$

$$\frac{\partial f\left(\hat{x}_k^{+}, u_k, \theta_k\right)}{\partial\hat{x}_k^{+}} = \begin{bmatrix} 1 & 0 & 0 & 0 & -u_k \\ 0 & \hat{\theta}_{3,k+1}^{-} - \hat{\theta}_{1,k+1}^{-}\hat{\theta}_{2,k+1}^{-} & 0 & 0 & 0 \\ 0 & 0 & \hat{\theta}_{6,k+1}^{-} - \hat{\theta}_{4,k+1}^{-}\hat{\theta}_{5,k+1}^{-} & 0 & 0 \\ 0 & 0 & 0 & 1 & 0 \\ 0 & 0 & 0 & 0 & 1 \end{bmatrix}. \tag{34}$$

On the basis of Eq. (17), we can get

$$\frac{d\hat{x}_k^+}{d\theta_k} = D_{k-1}^{\theta} - K_{k-1}^{x} H_{k-1}^{\theta}. \tag{35}$$

In Eq. (35), the initial values of D_k^{θ} and H_k^{θ}, i.e. D_0^{θ} and H_0^{θ}, are both zero. Therefore, we can get the value of $\frac{d\hat{x}_k^+}{d\theta_k}$, D_k^{θ} as well as H_k^{θ} by recursive calculation based on the above equations.

IV. EXPERIMENTAL AND PARAMETER IDENTIFICATION OF FRACTIONAL-ORDER MODEL

A. DESCRIPTION OF EXPERIMENTAL DATA

The raw data used in this paper to validate the proposed method are acquired from open-source datasets provided by the CALCE battery research group of University of Maryland. The battery test bench mainly consists of a charge-discharge test system for batteries (Arbin BT2000), a programmable thermal chamber for temperature control, and a monitoring PC with Arbins' Mits Pro Software installed. The professional software for battery test can control Arbin BT2000 and the thermal chamber. The detail description about the battery test bench refers to Ref. [33]. INR18650-20R lithium-ion battery manufactured by Samsung with a rated capacity of 2 Ah and a rated voltage of 3.6 V is used for the tests. By the test bench, the battery charge and discharge tests are conducted at different dynamic current profiles (FUDS, DST, US06 and the Hybrid Pulse Power Characteristic (HPPC)) and at different temperatures (0°C, 25°C and 45°C). The sampling time for all data collection is 1 s. In this study, we choose the current and voltage profiles at room temperature (25°C) as the experimental data.

B. ESTABLISHMENT OF THE OCV-SOC RELATIONSHIP

It is of high importance to determine the relationship between OCV and SOC for accurately estimating the battery SOC. Due to the electrochemical characteristics of lithium-ion batteries, the OCV can only be accurately measured after the battery has sufficient rest to reach equilibrium, which makes the OCV online measurement impractical. Nevertheless, it is a proven fact that there exists a certain relationship between OCV and SOC. Through HPPC experiment, we can obtain the OCV values under certain SOC values, and then get the relationship between OCV and SOC by fitting obtained discrete point data.

Fig. 3 shows the current and voltage profiles during the HPPC experiment. The battery is first fully charged to 100% SOC, second was discharged for 12 min using 0.5 C current followed 2 h relaxation, thus leading to 10% reduction of SOC. Third, the discharge and relaxation process is repeated until the SOC becomes zero. Finally, 11 groups of OCV-SOC data are obtained. We use these data to fit the relationship between OCV and SOC by the following equation:

$$OCV\,(SOC) = a_0 + \sum_{i=1}^{8} a_i \cdot SOC^i. \tag{36}$$

TABLE 1. Fitted coefficients for the OCV-SOC curve.

Coefficient	value
a_0	3.264
a_1	3.383
a_2	-21.363
a_3	111.156
a_4	-395.440
a_5	849.963
a_6	-1032.069
a_7	651.322
a_8	-166.040

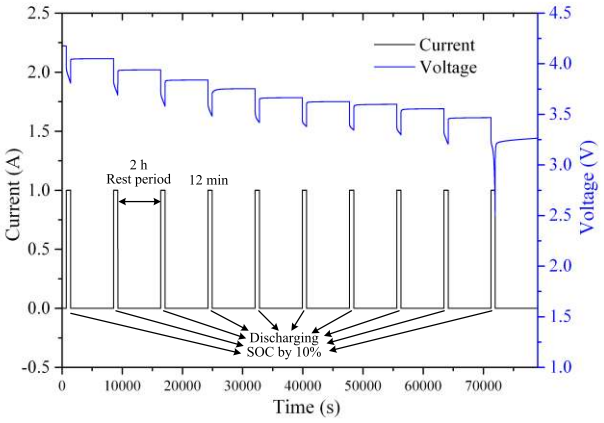

FIGURE 3. The current and voltage profiles of HPPC test.

The resulting fitting curve is shown in Fig. 4, and the fitted coefficients are listed in Table 1. As shown in Fig. 4, the experiment data are very close to the curve fitting, and the calculated root-mean square error (RMSE) is 2.6 mV.

In Refs. [27] and [34], another empirical formula was used to fit the relationship between OCV and SOC, as expressed by Eq. (37):

$$OCV\,(SOC) = a_0 + a_1 SOC + a_2 \frac{1}{SOC} + a_3 \ln(SOC) + a_4 \ln(1 - SOC). \tag{37}$$

We also use Eq. (37) to fit the relationship between OCV and SOC, and then calculate the RMSE as 7.1 mV. Obviously, it is preferable to use Eq. (36) to obtain the OCV-SOC relationship because the resulting RMSE based on Eq. (36) is much less than that based on Eq. (37).

C. IDENTIFICATION FOR THE INITIAL PARAMETER

As previously mentioned, the parameter of battery model is dealt with as constant value only with small perturbing noise, thus permitting small changes to be implemented to the value of the initial parameter. Therefore, to achieve convergence of the proposed DFOEKF algorithm as soon as possible, it is essential to identify the parameters of battery model offline in order to provide appropriate initial parameters for the algorithm.

In Refs. [25] and [29], genetic algorithm (GA) was demonstrated to be capable of identifying parameter of lithium-ion battery equivalent circuit model. However, ordinary GA is

TABLE 2. Parameter identification results for initialization.

Parameter	Value
R_0	0.160 Ω
R_1	0.301 Ω
R_2	0.345 Ω
C_1	1012 F
C_2	10333 F
α	0.892
β	0.825

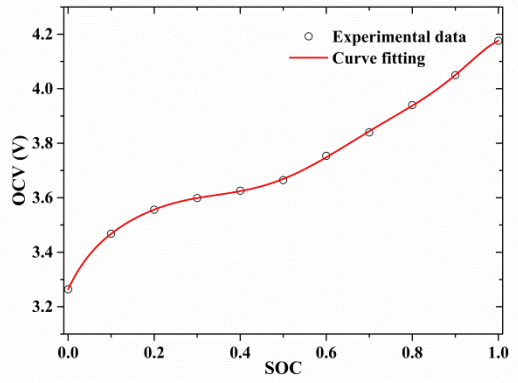

FIGURE 4. The OCV-SOC fitting curve.

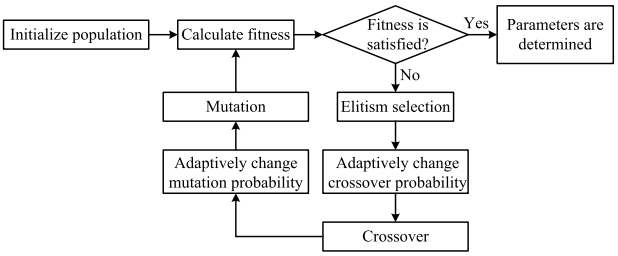

FIGURE 5. Flowchart of AGA for battery model parameter identification.

easy to fall into the local optimal solution, while adaptive genetic algorithm (AGA) has better global searching ability and faster convergence speed by using adaptive crossover and mutation probabilities. Therefore, we use AGA to identify the parameters of the fraction-order battery model, i.e. $R_0, R_1, C_1, R_2, C_2, \alpha$ and β. The AGA starts by randomly generating the individuals of the initial population. Each individual denotes a solution of the problem to be solved, and the elements composing the individuals are called genes. Each individual is a model parameter vector, and hence it is composed of seven genes denoting the values of (R_0, R_1, C_1, R_2, C_2, α and β). The fractional-order battery model is employed to calculate the battery terminal voltage, aiming to minimize the errors between measured terminal voltage and the terminal voltage resulting from the model. The detailed algorithm of AGA is shown in Fig. 5.

In this paper, HPPC current and voltage profiles in Fig. (3) are used to identify the parameters of battery model and the resulting parameter values are shown in Table 2.

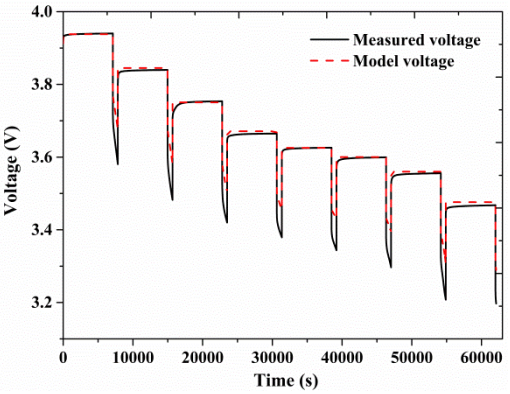

FIGURE 6. Measured voltage and model output voltage.

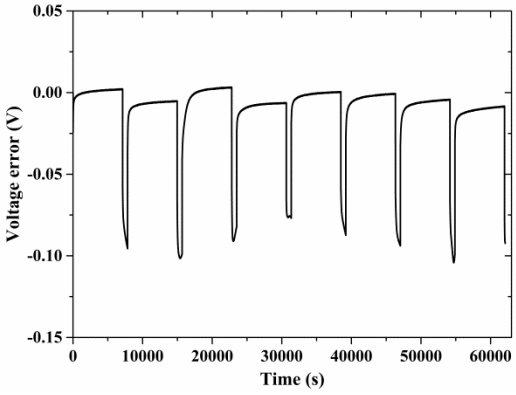

FIGURE 7. Error between measured voltage and model output voltage.

To verify the accuracy of parameter identification, we compare the model output terminal voltage and measured terminal voltage, as shown in Fig. 6. The voltage error is shown in Fig. 7. The calculated RMSE and mean absolute error (MAE) are 25.8 mV and 12.0 mV, respectively. These results verify the accuracy of parameter identification. It should be noted that the AGA is only used to get the appropriate initial values of model parameters for the DFOEKF, that is, the AGA only runs once before the SOC and SOH estimation.

V. RESULTS AND DISCUSSION

In order to verify the accuracy of the proposed algorithm, the battery SOC and SOH estimation are conducted under the FUDS, DST and US06 tests, respectively. Considering the impact of over-charge on battery life, the SOC of the battery is kept within 80% during all the tests. In addition, the impact of over-discharge should be taken into account. Therefore, the SOC/SOH estimation is operated under the condition of 10%-80% SOC.

A. ESTIMATION RESULTS AND ANALYSIS OF SOC

Under the HPPC test, although we have obtained the model parameters by offline identification method, these identified parameters are not necessarily suitable for the FUDS, DST and US06 tests. To make it clear and verify the accuracy

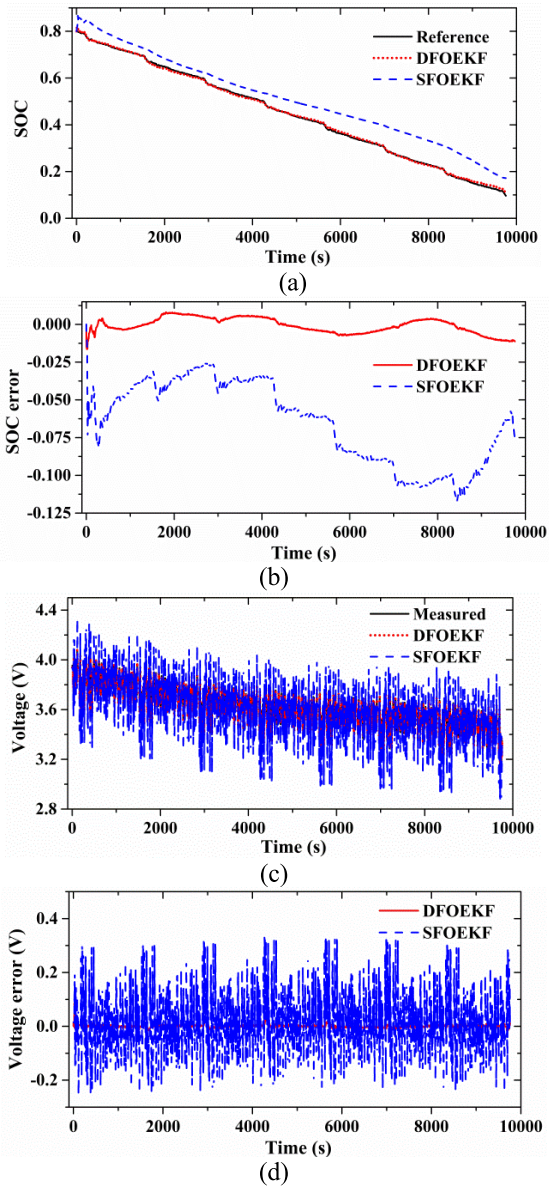

FIGURE 8. Comparisons of estimation results under the FUDS test: (a) SOC estimation results; (b) SOC errors; (c) voltage prediction results; (d) voltage errors.

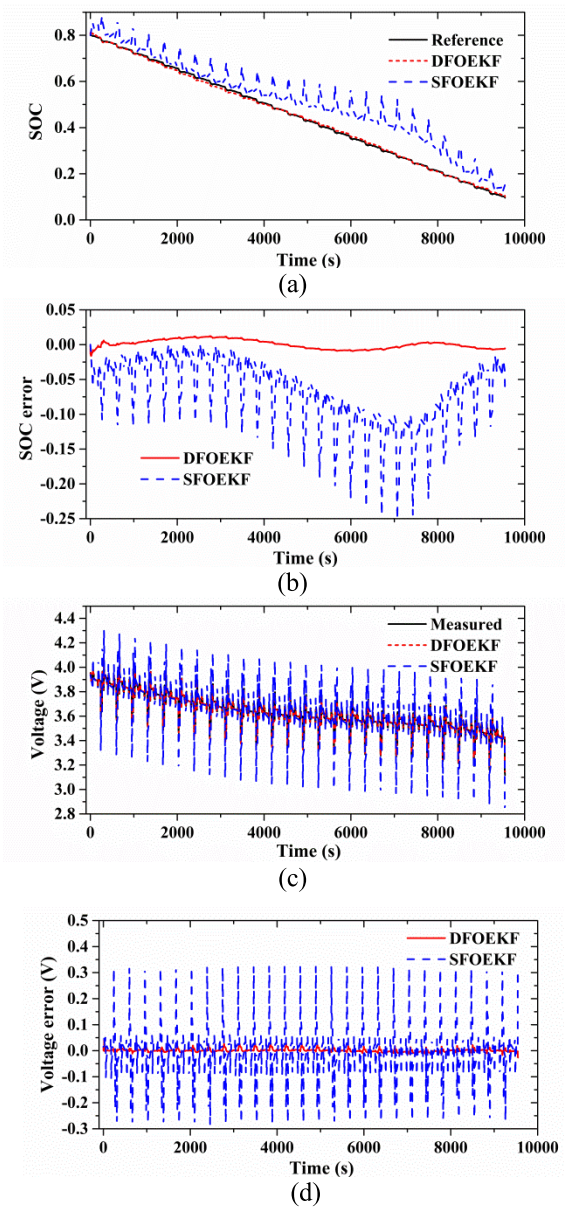

FIGURE 9. Comparisons of estimation results under the DST test: (a) SOC estimation results; (b) SOC errors; (c) voltage prediction results; (d) voltage errors.

of online parameter identification by the proposed method, we use a single fractional-order extended Kalman filter (is recorded as SFOEKF) and the proposed DFOEKF to estimate the SOC respectively, and then compare their estimation results. The SFOEKF is designed only for the SOC estimation. It uses the same battery model as the DFOEKF, and the model parameters are obtained under the HPPC test as shown in Table 2. These model parameters are fixed in the filtering process. The DFOEKF use the data in Table 2 to initialize the model parameters, and after initialization these parameters will be updated continuously in the filtering process. The SOC value calculated by coulomb counting method is regarded as the reference SOC. Before these two algorithms enter the iteration, both initial value of the SOC are set to be the correct value, namely, 0.8.

Fig. 8 (a) shows the comparisons of the battery SOC estimated by these two algorithms under the FUDS test. It can be observed that the SOC estimated by the DFOEKF are very close to the reference value, while the SOC estimated by the SFOEKF deviates from the reference value. The SOC estimation errors are shown in Fig. 8 (b). It can be seen that the SOC estimate error of the SFOEKF is much more than that of the DFOEKF. The resulted SOC RMSEs and MAEs estimated by the DFOEKF and SFOEKF are 0.48% and 0.41%, and 6.87% and 6.34%, respectively. These results indicate that there leads to a large SOC estimation error when using the model parameters identified under the HPPC test condition to estimate the SOC of the battery operated under the FUDS test condition, and on the other hand, the model

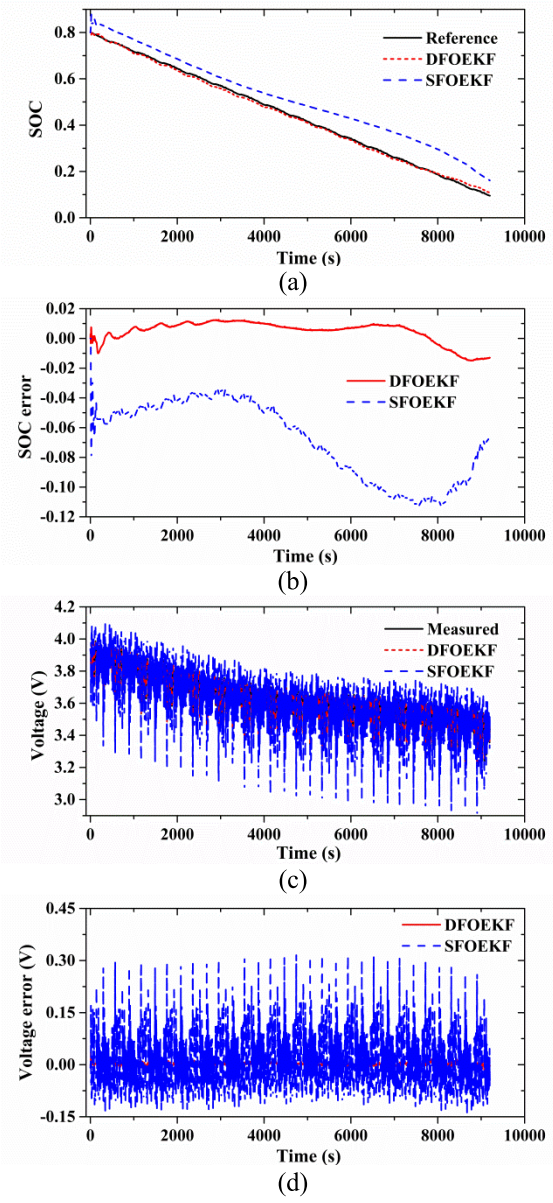

FIGURE 10. Comparisons of estimation results under the US06 test: (a) SOC estimation results; (b) SOC errors; (c) voltage prediction results; (d) voltage errors.

parameters are online identified accurately by the DFOEKF. To verify the accuracy of online parameter identification, we compare the prediction voltage and prediction error of these two algorithms, as shown in Fig. 8 (c) and (d). It can be seen that the voltage predicted by the DFOEKF is too close to the measured value almost to distinguish them. The voltage RMSE and MAE are only 4.9 mV and 3.4 mV, respectively. On the contrary, the voltage predicted by the SFOEKF deviates from the measured value, and the max voltage error exceeds 0.3 V. The voltage RMSE and MAE are 88.6 mV and 66.5 mV, respectively. The reason for such large voltage error is that the parameters identified under the HPPC test condition are not suitable for the FUDS test, while the DFOEKF resolves the issue by updating the parameters in the filtering process.

TABLE 3. Comparison of the SOC and voltage estimation errors.

Method	Test profile	SOC error (%) RMSE	SOC error (%) MAE	Voltage error (mV) RMSE	Voltage error (mV) MAE
DFOEKF	FUDS	0.48	0.41	4.9	3.4
	DST	0.63	0.54	5.7	3.8
	US06	0.86	0.79	3.8	3.0
FOEKF	FUDS	6.87	6.34	88.6	66.5
	DST	8.50	6.96	79.3	46.1
	US06	7.32	6.83	68.4	53.7

Fig. 9 (a)-(d) and Fig. 10 (a)-(d) show the comparisons of the battery SOC estimation and voltage prediction based on these two algorithms under the DST and US06 tests, respectively. It can be observed that both the SOC and voltage estimated by the DFOEKF can well match the reference SOC and measured voltage, respectively, whether the battery is operated under the DST or US06 test. The SOC and voltage errors under both test conditions are very small. The calculated RMSEs and MAEs of the SOC estimation and voltage prediction are shown in Table 3. The satisfactory results further verify the accuracy of the DFOEKF algorithm. On the contrary, both the SOC and voltage estimated by the SFOEKF still deviate from their respective reference value whether the battery is operated under the DST or US06 test. The SOC RMSEs under these two test conditions are 8.50% and 7.32%, respectively, and the voltage RMSEs are 79.3 mV and 68.4 mV, respectively. Specifically, under the DST test, there are some peaks of the SOC estimation error at the time when the discharge current suddenly increases or decreases. This result is caused by the battery polarization effect; thus, the instant change in discharge current results in a sudden change in the battery model parameters, which leads to large SOC errors. However, the SOC error estimated by the DFOEKF is still small due to online parameter update. These results indicate that it is inadvisable to use the model parameters identified under the HPPC test to estimate the SOC of the battery operated under the FUDS, DST and US06 tests unless the model parameters are updated online.

B. ESTIMATION RESULTS AND ANALYSIS OF SOH

Fig. 11 (a)-(c) show estimation results of the ohmic internal resistance R_0 under the FUDS, DST and US06 tests, respectively. To evaluate the estimation performance, we use AGA algorithm to identify R_0 offline under these three test conditions, respectively, and the resulted R_0 values are 0.0711 Ω, 0.0728 Ω and 0.0753 Ω, respectively. These identification results of R_0 are all very close to the value of 0.071 Ω reported in Ref. [33], hence they are regarded as the reference. From Fig. 11 (a)-(c), it can be seen that all the R_0 drop rapidly from the initial value (i.e. 0.16 Ω) to near the reference value and then oscillate around the reference value. The phenomenon of slight fluctuation below ±5% reference value confirms the fact that the ohmic internal resistance of the battery is slow variable and demonstrates the accuracy of R_0 estimation.

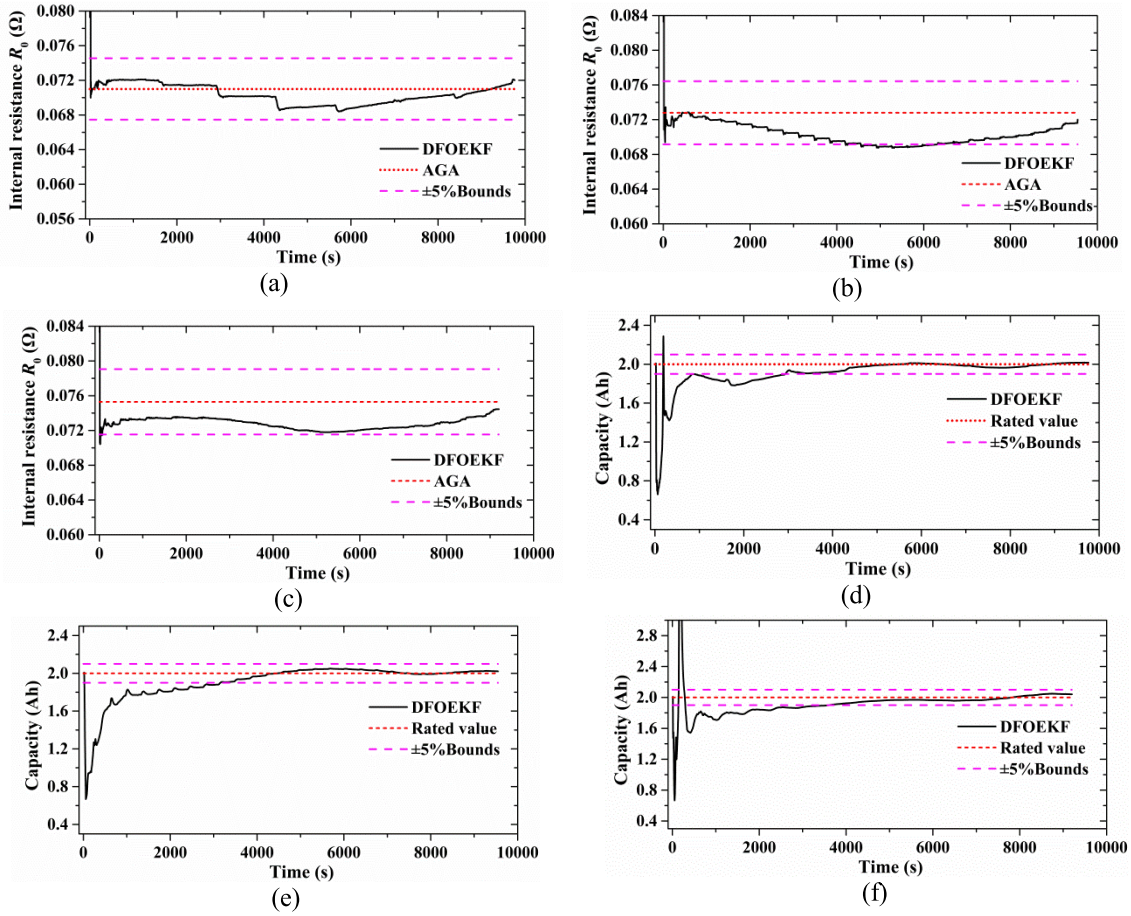

FIGURE 11. Estimation results of the ohmic internal resistance R_0 and the capacity C_P: (a) R_0 estimation under the FUDS test; (b) R_0 estimation under the DST test; (c) R_0 estimation under the US06 test; (d) C_p estimation under the FUDS test; (e) C_p estimation under the DST test; (f) C_p estimation under the US06 test.

Fig. 11 (d)-(f) show estimation results of the capacity C_p under the FUDS, DST and US06 tests, respectively. It can be observed that there is a large oscillation at the beginning of discharge, but after the initial stage (Time >800 s), C_p fluctuates slightly due to a slow variable of battery capacity, and finally all the estimated capacity converge toward the rated value reasonably. The steady-state estimation errors in the capacity are bounded by 5%. R_0 and C_p estimation results demonstrate the effectiveness of the proposed DFOEKF algorithm. It should be noted that the SOH estimation at the different aging levels of the battery should be conducted in order to further verify its effectiveness. Unfortunately, there are no related open-source data provided by the CALCE research group. Nevertheless, the accuracy of the SOH estimation for fresh battery operated under the FUDS, DST and US06 tests has been validated.

C. VERIFICATION OF THE ALGORITHM CONVERGENCE

It is difficult to obtain accurate initial value of the variables (i.e. the SOC, ohmic internal resistance R_0 and capacity C_p of the battery) to be estimated for a BMS. Therefore, it is necessary to verify the convergence and robustness of the proposed method in the case of unknown initial value of the variables to be estimated. As shown in Table 4, the initial SOC values are set to 0.9 and 0.6, respectively, and we record these two cases as IS-1 and IS-2, respectively. The initial R_0 values are set to 150% $R_{0,id}$ and 50% $R_{0,id}$, respectively, and we record these two cases as IS-3 and IS-4, respectively. The initial C_p values are set to 150% $C_{p,r}$ and 50% $C_{p,r}$, respectively, and we record these two cases as IS-5 and IS-6, respectively.

TABLE 4. Six cases with different initial values of the state.

Case name	Initial state		
	SOC(0)	$R_0(0)$ (Ω)	$C_P(0)$ (Ah)
IS-1	0.9	$R_{0,id}$	$C_{p,r}$
IS-2	0.6	$R_{0,id}$	$C_{p,r}$
IS-3	0.8	150% $R_{0,id}$	$C_{p,r}$
IS-4	0.8	50% $R_{0,id}$	$C_{p,r}$
IS-5	0.8	$R_{0,id}$	150% $C_{p,r}$
IS-6	0.8	$R_{0,id}$	50% $C_{p,r}$

Where $R_{0,id}$ denotes the value of R_0 in Table 2, and $C_{p,r}$ represents the rated capacity.

Fig. 12 (a)-(b), Fig. 13 (a)-(b) and Fig. 14 (a)-(b) show the SOC estimation results in the six cases under the FUDS, DST and US06 tests, respectively. It can be seen that all the

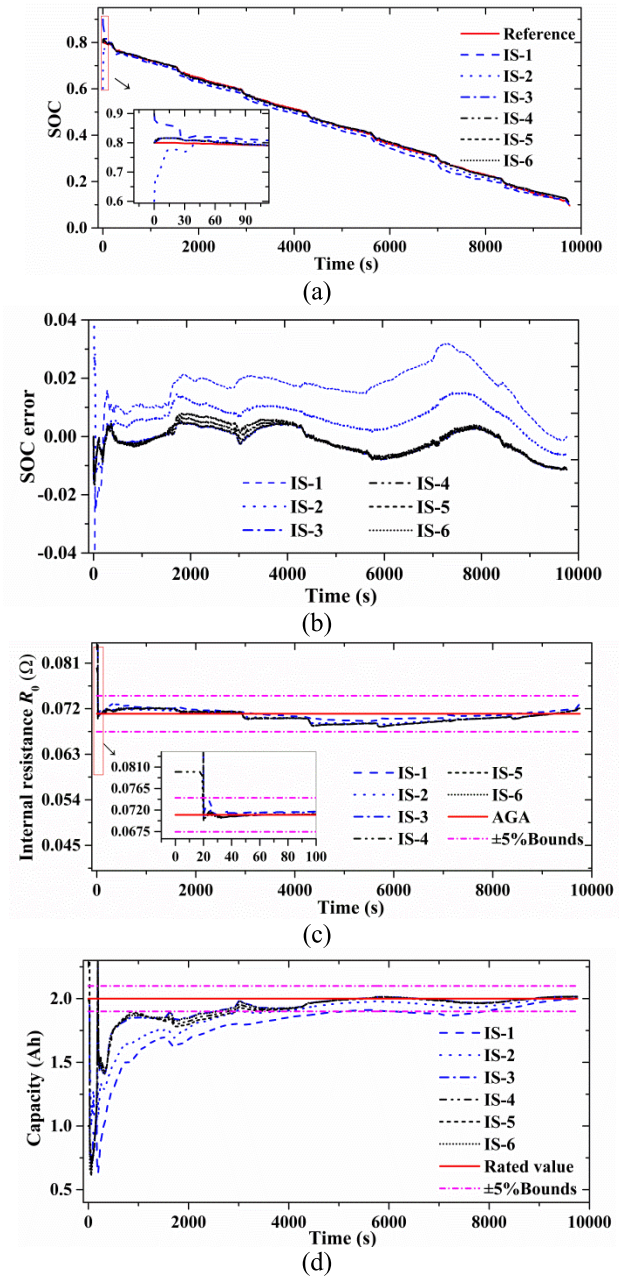

FIGURE 12. Estimation results in six cases under the FUDS test: (a) SOC estimation results; (b) SOC errors; (c) R_0 estimation results; (d) C_p estimation results.

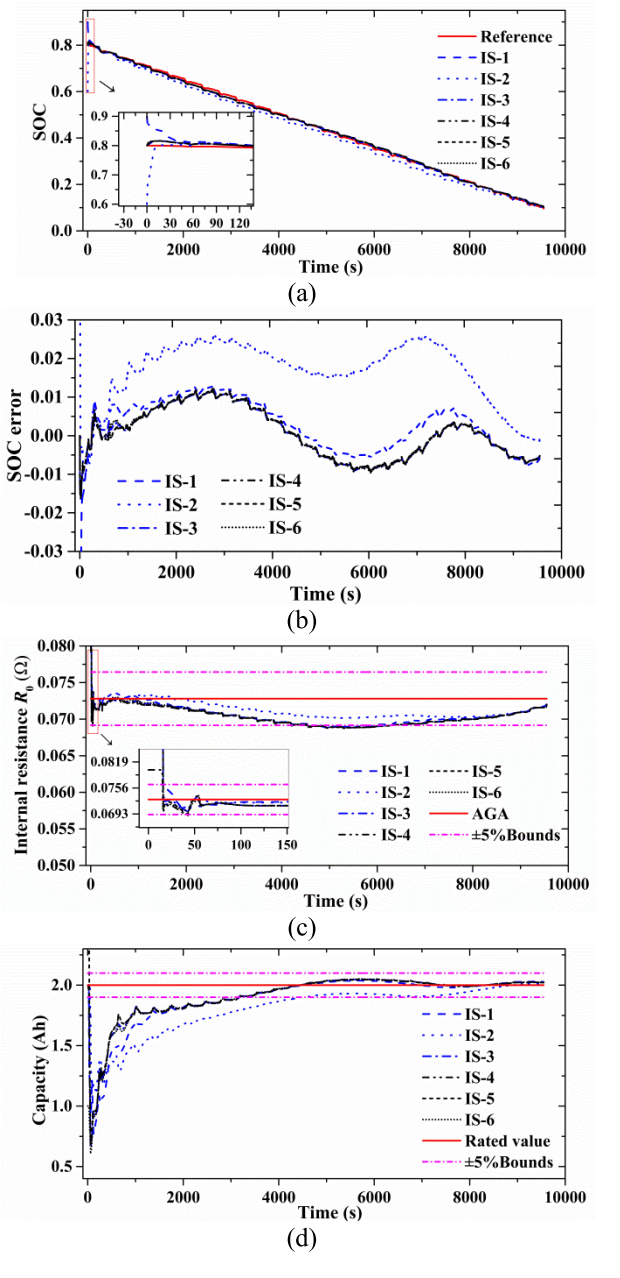

FIGURE 13. Estimation results in six cases under the DST test: (a) SOC estimation results; (b) SOC errors; (c) R_0 estimation results; (d) C_p estimation results.

SOC curves can rapidly track the reference curve. In IS-1 and IS-2 cases, the estimated SOC reaches 95% reference value within 30 s from the initial value of 0.9 and 0.6, respectively, and matches with the reference well after time >30 s. In other cases, the estimated SOC keeps consistent with the reference all the time. The calculated SOC RMSEs and MAEs as well as voltage RMSEs and MAEs in all cases are shown in Table 5. It can be observed that wrong SOC initial value has the most influence on the SOC estimation. Nevertheless, this influence is only significant in the initial stage of the estimation and then becomes negligible. In Ref. [35], a robust estimator based on maximum exponential absolute value was presented and had good robustness even though gross errors or bad data points exist, but not for the SOC estimation.

Fig. 12 (c), Fig. 13 (c) and Fig. 14 (c) show R_0 estimation results in the six cases under the FUDS, DST and US06 tests, respectively. It can be seen that all the estimated R_0 oscillate around the reference curve. The steady-state estimation errors are bounded by 5%. In IS-3 case, the estimated R_0 can rapidly drop back to near the reference curve even though the initial value (0.24 Ω) is several times of the reference value.

Fig. 12 (d), Fig. 13 (d) and Fig. 14 (d) show C_p estimation results in the six cases under the FUDS, DST and US06 tests, respectively. It can be observed that all the estimated C_p

TABLE 5. SOC and voltage estimation errors in six cases under the FUDS, DST and US06 tests.

Test profile	Case name	SOC error (%) RMSE	SOC error (%) MAE	Voltage error (mV) RMSE	Voltage error (mV) MAE
FUDS	IS-1	2.03	1.88	5.4	4.4
	IS-2	1.04	0.89	5.2	3.4
	IS-3	0.40	0.33	5.3	3.4
	IS-4	0.44	0.37	4.9	3.4
	IS-5	0.48	0.41	4.9	3.4
	IS-6	0.40	0.34	5.1	3.4
DST	IS-1	0.75	0.61	5.7	3.8
	IS-2	1.88	1.71	5.7	4.2
	IS-3	0.64	0.55	5.8	3.8
	IS-4	0.63	0.54	5.7	3.8
	IS-5	0.63	0.54	5.7	3.8
	IS-6	0.64	0.55	5.7	3.8
US06	IS-1	1.00	0.62	4.5	3.3
	IS-2	1.06	0.88	4.5	2.9
	IS-3	0.93	0.87	3.9	3.0
	IS-4	0.80	0.72	3.8	2.9
	IS-5	0.89	0.82	3.9	3.2
	IS-6	0.79	0.71	3.8	2.9

converge toward the rated value reasonably although there is a large oscillation in the initial stage of estimation. The steady-state estimation errors are bounded by 5%. In IS-5 and IS-6 cases, the convergence of C_p estimation is not destroyed by initial error of 50%. The estimation results of the SOC, R_0 and C_p in the case of wrong initial value demonstrate the convergence and robustness of the proposed method.

As previous discussion, we have successfully used the joint FOEKF estimator to estimate the SOC and SOH synchronously. Nonetheless, Ref. [36] indicates that this joint EKF may be subject to stability problem due to its adaptive structure. Theoretically, it is still very difficult to derive a proof of stability for this type of estimator. However, Ref. [36] also demonstrates that if model parameters are slowly varying adequately, joint EKF is stable in most cases. For the application of lithium-ion batteries state estimation, the ohmic internal resistance and battery capacity meet this slowly-varying requirement very well, which has a marginal adverse influence on the EKF stability, leading to a convergent estimator.

D. ESTIMATION RESULTS WITH DIFFERENT CURRENT AND VOLTAGE NOISES

In the actual application, the sensors for measuring the terminal voltage of the battery and load current are often interfered by the working environment, for example electro-magnetic interference, which results in measurement errors in the voltage and current. Inaccurate voltage and current will affect the SOC and SOH estimation accuracy. Therefore, different noises are added to the measured voltage current to test and verify the robustness of the proposed method.

First, the current errors from −30 mA to 30 mA (with the interval of 5 mA) are imposed on the measured current. Fig. 15 shows the change of SOC estimation and voltage prediction error with the twelve current errors under the FUDS, DST and US06 tests. Second, the voltage errors from −30 mV to 30 mV (with the interval of 5 mV) are imposed

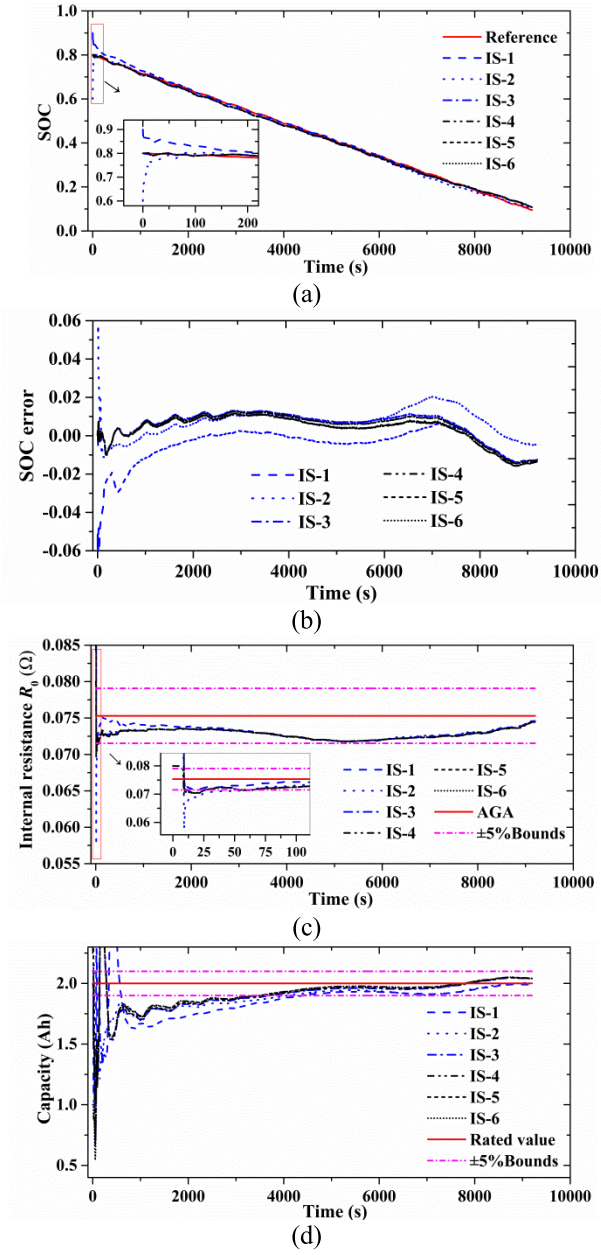

FIGURE 14. Estimation results in six cases under the US06 test: (a) SOC estimation results; (b) SOC errors; (c) R_0 estimation results; (d) C_p estimation results.

on the measured voltage. Fig. 16 shows the change of SOC estimation and voltage prediction error with the twelve voltage errors under the FUDS, DST and US06 tests. It can be seen that SOC estimation error increases with the increase of current and voltage error. It is also found that current error has a marginal influence on voltage prediction. This is because the ohmic internal resistance of the battery is very small, which leads to a small voltage change. In addition, current error has a less influence on the SOC estimation than voltage error. On the contrary, voltage error has a considerable influence on the results, especially the SOC estimation. Therefore, the accuracy of the voltage sensor should be ensured as much

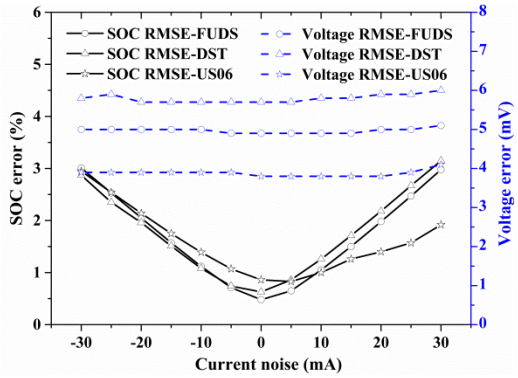

FIGURE 15. Change of SOC and voltage estimation errors with different current noises.

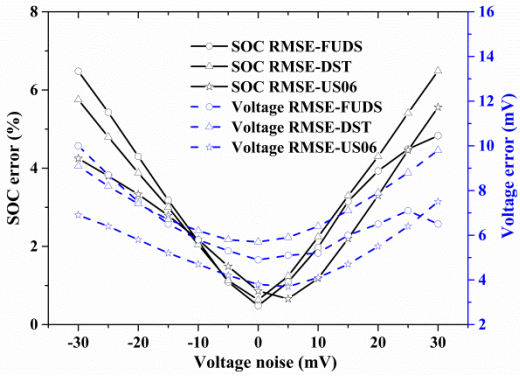

FIGURE 16. Change of SOC and voltage estimation errors with different voltage noises.

TABLE 6. SOC and voltage estimation errors under the FUDS, DST and US06 tests at different temperature.

Test profile	Temperature	SOC error (%) RMSE	SOC error (%) MAE	Voltage error (mV) RMSE	Voltage error (mV) MAE
FUDS	0 ℃	1.27	0.99	5.9	4.0
	25 ℃	0.48	0.41	4.9	3.4
	45 ℃	0.50	0.38	3.6	2.6
DST	0 ℃	1.61	1.20	7.1	5.3
	25 ℃	0.63	0.54	5.7	3.8
	45 ℃	0.38	0.30	3.8	2.8
US06	0 ℃	1.73	1.48	8.0	4.6
	25 ℃	0.86	0.79	3.8	3.0
	45 ℃	0.49	0.43	3.2	2.5

as possible. It should be noted that there have already been proposed estimation methods in other applications that ensure the robustness even in the case of noisy data [37], [38]. These methods may be used to improve the robustness of SOC estimation if an appropriate battery model is built.

Voltage and current errors have also certain influence on the estimation of R_0 and C_p. If we can ensure the voltage error less than 10 mV or current error less than 20 mA, the steady-state estimation error of R_0 and C_p is still bounded by 5% whether the battery is operate under the FUDS, DST or US06 test.

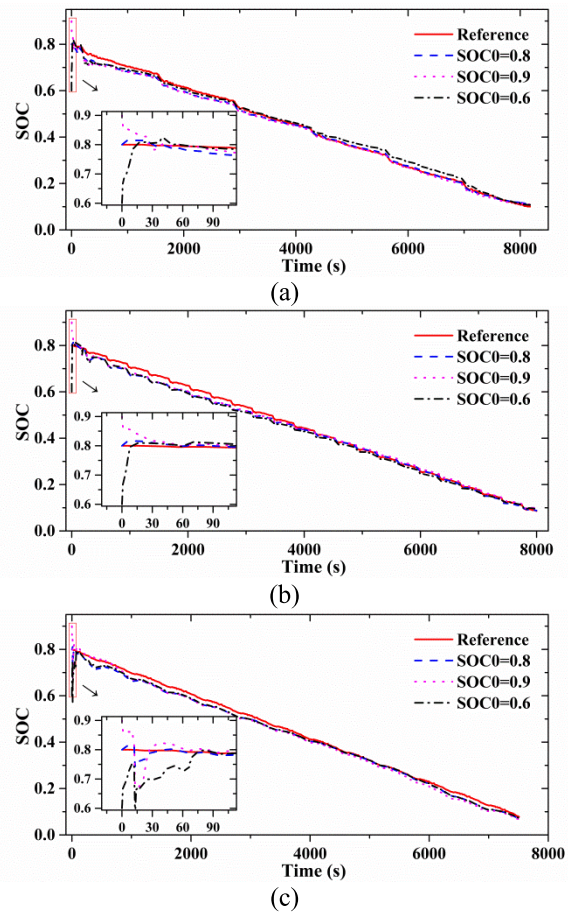

FIGURE 17. SOC Estimation results under different initial SOC values at 0 °C: (a) under the FUDS test; (b) under the DST test; (c) under the US06 test.

E. ESTIMATION RESULTS AT DIFFERENT TEMPERATURES

Fig. 17 (a)-(c) and Fig. 18 (a)-(c) show the SOC estimation results at the temperatures of 0 °C and 45 °C, respectively. It can be seen that all the SOC curves can rapidly track the reference curve under different initial SOC values. The calculated RMSEs and MAEs of the SOC estimation and voltage prediction under correct initial SOC value are shown in Table 6. The SOC estimation accuracy is the worst at 0 °C, which is owing to poor performance of the battery at low temperature. Nevertheless, all the RMSEs and MAEs of the SOC estimation under the FUDS, DST and US06 tests are less than 2%. For SOH estimation, both relative estimation errors in R_0 and the capacity are still less than 5% whether the battery is operated at 0 °C or 45 °C. These results demonstrate the robustness, convergence and accuracy of the proposed method applied at different temperatures.

F. COMPUTATIONAL COMPLEXITY OF THE ALGORITHM

Low computational complexity is required for the real-time application. The proposed algorithm written in MATLAB R2018a is executed on a system with Intel(R) Core(TM) i7-6600U CPU @ 2.6 GHz and 8 GB of RAM. Average running time of the algorithm is about 0.76 s for 9760 sample points.

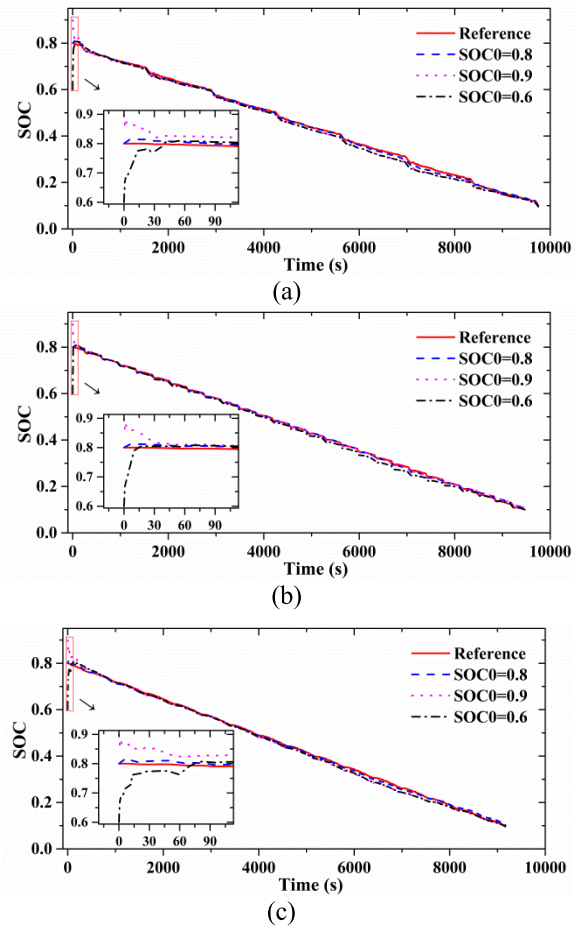

FIGURE 18. SOC Estimation results under different initial SOC values at 45 °C: (a) under the FUDS test; (b) under the DST test; (c) under the US06 test.

VI. CONCLUSION

In this paper, a fractional second-order RC circuit is employed to model the battery, and based on the model a DFOEKF algorithm is proposed for co-estimation of the SOC and SOH as well as online parameter identification. The offline parameter identification of the battery model is implemented using AGA algorithm under the HPPC test and the accuracy of the parameter identification is validated. A SFOEKF algorithm based on the offline identified parameters is also used to estimate the SOC. Comparisons of the SOC estimation results using the DFOEKF and the SFOEKF under the FUDS, DST and US06 tests are performed. The results show that the DFOEKF can obtain more accurate SOC value by updating the model parameters online than the SFOEKF with fixed parameters. The SOC RMSEs decrease from 6.87%, 8.50% and 7.32% to 0.48%, 0.63% and 0.86% under the FUDS, DST and US06 tests, respectively at room temperature. In addition, the model becomes more accurate by updating the model parameters online. The model voltage RMSEs decrease from 88.6 mV, 79.3 mV and 68.4 mV to 4.9 mV, 5.7 mV and 3.8 mV, respectively. The estimation accuracy of ohmic internal resistance and the capacity is also verified under these three tests. Finally, the convergence and robustness of the proposed method are discussed and verified by using the wrong initial state value and noise analysis.

REFERENCES

[1] L. Zhang, X. Hu, Z. Wang, J. Ruan, C. Ma, Z. Song, D. G. Dorrell, and M. G. Pecht, "Hybrid electrochemical energy storage systems: An overview for smart grid and electrified vehicle applications," *Renew. Sustain. Energy Rev.*, vol. 139, Apr. 2021, Art. no. 110581.

[2] Q. Wang, Z. Wang, L. Zhang, P. Liu, and Z. Zhang, "A novel consistency evaluation method for series-connected battery systems based on real-world operation data," *IEEE Trans. Transp. Electrific.*, early access, Aug. 20, 2020, doi: 10.1109/TTE.2020.3018143.

[3] J. Meng, M. Ricco, G. Luo, M. Swierczynski, D.-I. Stroe, A.-I. Stroe, and R. Teodorescu, "An overview and comparison of online implementable SOC estimation methods for lithium-ion battery," *IEEE Trans. Ind. Appl.*, vol. 54, no. 2, pp. 1583–1591, Mar. 2018.

[4] Z. Li, M. Lin, and C. Yong, "Least-squares based Coulomb counting method and its application for state-of-charge (SOC) estimation in electric vehicles," *Int. J. Energy Res.*, vol. 40, no. 10, pp. 1389–1399, Aug. 2016.

[5] Y. Xing, W. He, M. Pecht, and K. L. Tsui, "State of charge estimation of lithium-ion batteries using the open-circuit voltage at various ambient temperatures," *Appl. Energy*, vol. 113, pp. 106–115, Jan. 2014.

[6] L. Kang, X. Zhao, and J. Ma, "A new neural network model for the state-of-charge estimation in the battery degradation process," *Appl. Energy*, vol. 121, pp. 20–27, May 2014.

[7] T. Weigert, Q. Tian, and K. Lian, "State-of-charge prediction of batteries and battery–supercapacitor hybrids using artificial neural networks," *J. Power Sources*, vol. 248, no. 2, pp. 1028–1033, Feb. 2014.

[8] W. X. Shen, "State of available capacity estimation for lead-acid batteries in electric vehicles using neural network," *Energy Convers. Manage.*, vol. 48, no. 2, pp. 433–442, Feb. 2007.

[9] B. Cheng, Y. L. Zhou, J. X. Zhang, J. P. Wang, and B. G. Cao, "Ni–MH batteries state-of-charge prediction based on immune evolutionary network," *Energy Convers. Manage.*, vol. 50, no. 12, pp. 3078–3086, Dec. 2009.

[10] V. Klass, M. Behm, and G. Lindbergh, "Capturing lithium-ion battery dynamics with support vector machine-based battery model," *J. Power Sources*, vol. 298, no. 12, pp. 92–101, Dec. 2015.

[11] C. Hametner and S. Jakubek, "State of charge estimation for lithium ion cells: Design of experiments, nonlinear identification and fuzzy observer design," *J. Power Sources*, vol. 238, pp. 413–421, Sep. 2013.

[12] D. Kim, T. Goh, M. Park, and S. Kim, "Fuzzy sliding mode observer with grey prediction for the estimation of the state-of-charge of a lithium-ion battery," *Energies*, vol. 8, no. 11, pp. 12409–12428, Nov. 2015.

[13] Q. Zhu, L. Li, X. S. Hu, N. Xiong, and G. D. Hu, "H_∞-based nonlinear observer design for state of charge estimation of lithium-ion battery with polynomial parameters," *IEEE Trans. Veh. Technol.*, vol. 66, no. 12, pp. 10853–10865, Dec. 2017.

[14] A. Tulsyan, Y. Tsai, R. B. Gopaluni, and R. D. Braatz, "State-of-charge estimation in lithium-ion batteries: A particle filter approach," *J. Power Sources*, vol. 331, pp. 208–223, Nov. 2016.

[15] C. Huang, Z. Wang, Z. Zhao, L. Wang, C. S. Lai, and D. Wang, "Robustness evaluation of extended and unscented Kalman filter for battery state of charge estimation," *IEEE Access*, vol. 6, pp. 27617–27628, Jun. 2018.

[16] D. Sun, X. Yu, C. Wang, C. Zhang, R. Huang, Q. Zhou, T. Amietszajew, and R. Bhagat, "State of charge estimation for lithium-ion battery based on an intelligent adaptive extended Kalman filter with improved noise estimator," *Energy*, vol. 214, Jan. 2021, Art. no. 119025.

[17] J. Lv, B. Jiang, X. Wang, Y. Liu, and Y. Fu, "Estimation of the state of charge of lithium batteries based on adaptive unscented Kalman filter algorithm," *Electronics*, vol. 9, no. 9, p. 1425, Sep. 2020.

[18] C. She, Z. Wang, F. Sun, P. Liu, and L. Zhang, "Battery aging assessment for real-world electric buses based on incremental capacity analysis and radial basis function neural network," *IEEE Trans. Ind. Informat.*, vol. 16, no. 5, pp. 3345–3354, May 2020.

[19] Y. Zou, X. Hu, H. Ma, and S. E. Li, "Combined state of charge and state of health estimation over lithium-ion battery cell cycle lifespan for electric vehicles," *J. Power Sources*, vol. 273, pp. 793–803, Jan. 2015.

[20] N. Wassiliadis, J. Adermann, A. Frericks, M. Pak, C. Reiter, B. Lohmann, and M. Lienkamp, "Revisiting the dual extended Kalman filter for battery state-of-charge and state-of-health estimation: A use-case life cycle analysis," *J. Energy Storage*, vol. 19, pp. 73–87, Oct. 2018.

[21] K. Yang, Z. Chen, Z. He, Y. Wang, and Z. Zhou, "Online estimation of state of health for the airborne li-ion battery using adaptive DEKF-based fuzzy inference system," *Soft Comput.*, vol. 24, no. 24, pp. 18661–18670, Jul. 2020.
[22] W. X. Duan, C. X. Song, Y. Chen, F. Xiao, S. L. Peng, Y. L. Shao, and S. X. Song, "Online parameter identification and state of charge estimation of battery based on multitimescale adaptive double Kalman filter algorithm," *Math. Problems Eng.*, vol. 2020, no. 12, Dec. 2020, Art. no. 9502605.
[23] R. Xiao, J. Shen, X. Li, W. Yan, E. Pan, and Z. Chen, "Comparisons of modeling and state of charge estimation for lithium-ion battery based on fractional order and integral order methods," *Energies*, vol. 9, no. 3, p. 184, Mar. 2016.
[24] K. S. R. Mawonou, A. Eddahech, D. Dumur, D. Beauvois, and E. Godoy, "Improved state of charge estimation for li-ion batteries using fractional order extended Kalman filter," *J. Power Sources*, vol. 435, Sep. 2019, Art. no. 226710.
[25] Q. Zhu, M. Xu, W. Liu, and M. Zheng, "A state of charge estimation method for lithium-ion batteries based on fractional order adaptive extended Kalman filter," *Energy*, vol. 187, Nov. 2019, Art. no. 115880.
[26] Y. Chen, D. Huang, Q. Zhu, W. Liu, C. Liu, and N. Xiong, "A new state of charge estimation algorithm for lithium-ion batteries based on the fractional unscented Kalman filter," *Energies*, vol. 10, no. 9, p. 1313, Sep. 2017.
[27] Y. Xu, M. Hu, A. Zhou, Y. Li, S. Li, C. Fu, and C. Gong, "State of charge estimation for lithium-ion batteries based on adaptive dual Kalman filter," *Appl. Math. Model.*, vol. 77, no. 1, pp. 1255–1272, Jan. 2020.
[28] X. Hu, H. Yuan, C. Zou, Z. Li, and L. Zhang, "Co-estimation of state of charge and state of health for lithium-ion batteries based on fractional-order calculus," *IEEE Trans. Veh. Technol.*, vol. 67, no. 11, pp. 10319–10329, Nov. 2018.
[29] M. Cai, W. Chen, and X. Tan, "Battery state-of-charge estimation based on a dual unscented Kalman filter and fractional variable-order model," *Energies*, vol. 10, no. 10, p. 1577, Oct. 2017.
[30] D. Zhou, K. Zhang, A. Ravey, F. Gao, and A. Miraoui, "Parameter sensitivity analysis for fractional-order modeling of lithium-ion batteries," *Energies*, vol. 9, no. 3, pp. 123–148, Feb. 2016.
[31] I. Petras, "Frational calculus," in *Frational-Order Nonlinear Systems: Modeling, Analysis and Simulation*. Berlin, Germany: Springer, 2011, pp. 9–12.
[32] R. G. G. Caponetto Dongola, L. L. Frotuna, and I. Petras, "Field programmable gate array implementation," in *Fractional Order Systems: Modeling and Control Applications*. Singapore: World Scientific, 2010, pp. 81–82.
[33] F. Zheng, Y. Xing, J. Jiang, B. Sun, J. Kim, and M. Pecht, "Influence of different open circuit voltage tests on state of charge online estimation for lithium-ion batteries," *Appl. Energy*, vol. 183, pp. 513–525, Dec. 2016.
[34] G. L. Plett, "Extended Kalman filtering for battery management systems of LiPB-based HEV battery packs: Part 2. Modeling and identification," *J. Power Sources*, vol. 134, no. 2, pp. 262–276, Aug. 2004.
[35] Y. Chen, J. Ma, P. Zhang, F. Liu, and S. Mei, "Robust state estimator based on maximum exponential absolute value," *IEEE Trans. Smart Grid*, vol. 8, no. 4, pp. 1537–1544, Jul. 2017.
[36] P. A. Ioannou and J. Sun, "Robust adaptive laws," in *Robust Adaptive Control*. New York, NY, USA: Dover, 2012, pp. 531–624.
[37] Y. Chen, Y. Yao, and Y. Zhang, "A robust state estimation method based on SOCP for integrated electricity-heat system," *IEEE Trans. Smart Grid*, vol. 12, no. 1, pp. 810–820, Jan. 2021.
[38] Y. Chen, F. Liu, S. Mei, and J. Ma, "A robust WLAV state estimation using optimal transformations," *IEEE Trans. Power Syst.*, vol. 30, no. 4, pp. 2190–2191, Jul. 2015.

LIUYI LING received the Ph.D. degree in optics from the University of Chinese Academy of Sciences, Hefei, China, in 2013. He is currently a Professor with the Anhui University of Science and Technology, Huainan, China. His current research interests include detection technology and information processing technology.

YING WEI received the master's degree in electrical engineering from the Anhui University of Science and Technology, Huainan, China, in 2007. She is currently an Associate Professor with Anhui Sanlian University, Hefei, China. Her current research interests include state estimation of lithium-ion batteries and safety monitoring technology.